Journal of Power Sources 221 (2013) 201–209

Contents lists available at SciVerse ScienceDirect

Journal of Power Sources

journal homepage: www.elsevier.com/locate/jpowsour

Electrical model to predict current–voltage behaviours of lithium ferro phosphate batteries using a transient response correction method

W.Y. Low [a], J.A. Aziz [a,*], N.R.N. Idris [a], R. Saidur [b]

[a] Department of Energy Conversion, Faculty of Electrical Engineering, Universiti Teknologi Malaysia, 81300 Skudai, Johor, Malaysia
[b] Department of Mechanical Engineering, University of Malaya, 50603 Kuala Lumpur, Malaysia

HIGHLIGHTS

- We model $LiFePO_4$ battery with new electrical model.
- Parameters in battery model are divided into loaded and unloaded conditions.
- Transient response correction is proposed to formulate the parameters.
- We validate the proposed battery model with experiment.

ARTICLE INFO

Article history:
Received 29 May 2012
Received in revised form
16 July 2012
Accepted 31 July 2012
Available online 23 August 2012

Keywords:
Lithium-ion batteries
Lithium ferro phosphate
Electrical battery model
Energy storage
Rechargeable battery characterisation

ABSTRACT

Lithium ferro phosphate ($LiFePO_4$) batteries are stable in terms of their thermal and chemical characteristics and have a high potential for wide use in the future. A battery model that predicts current–voltage (I–V) performance with high accuracy is vital for circuit designers so they can design circuits to control the usage of the battery and improve its runtime and its safety during use. In this paper, a battery model with two resistance–capacitance (RC) parallel networks is used for modelling and the values for parameters are divided into two sets; one for loaded conditions and the other for unloaded conditions. A methodology of transient response correction is proposed for formulating the parameters of the loaded condition. The steps for parameter extraction are discussed and the proposed battery model is validated using data from several experiments. The comparison between experiment and simulation results shows that the proposed model is capable of predicting I–V performance of the battery with very little error.

1. Introduction

Rechargeable batteries have been utilized as an energy storage element for portable electronic devices, electric vehicles and distributed generation and avionics systems. The lithium-ion battery has been the dominant type used in portable electronic devices due to its high specific energy and the compact size [1]. The lithium ferro phosphate ($LiFePO_4$) battery, which uses phosphate as its cathode, is expected to be widely used as the energy storage element in the future due to its advantages in thermal and chemical stability [2].

Even though battery technology has significantly improved in recent years, modern batteries are still unable to meet the energy demands of current portable electronic devices [3,4]. Therefore, battery management is important for battery-powered devices because it reduces power dissipation and extends the operation time of the battery. In order to have an effective battery management system for a $LiFePO_4$ battery, the development of a model that can accurately predict its dynamic behaviours is crucial [5].

There have been remarkable efforts committed to the development of battery models over the past decades. The three categories of battery models are electrochemical models, mathematical models and electrical models. Because the electrochemical models have high complexity and the mathematical models are unable to provide I–V information, these models are not well suited to use by circuit designers [3]. The electrical model is one that can be applied fairly easily by circuit designers because the mathematical

* Corresponding author. Tel.: +60 7 5535341; fax: +60 7 5566272.
E-mail address: junaidi@fke.utm.my (J.A. Aziz).

0378-7753/$ – see front matter © 2012 Elsevier B.V. All rights reserved.
http://dx.doi.org/10.1016/j.jpowsour.2012.07.140

Nomencalture

List of symbols

γ	state-of-charge of battery, %
C_N	nominal capacity of battery, Ah
R_{sr}	series resistance for full charged battery, Ω
R_a	increment of series resistance, Ω
R_1 and R_2	resistances for RC parallel networks during loaded conditions, Ω
R'_1 and R'_2	resistances for RC parallel networks during unloaded conditions, Ω
V_t	terminal voltage of battery, V
V_{k1} and V_{k2}	voltage across first RC parallel networks during loaded conditions, V
V'_{k1} and V'_{k2}	voltage across first RC parallel networks during unloaded conditions, V
τ_{k1} and τ_{k2}	time constants of the transient response during loaded conditions, s
τ'_{k1} and τ'_{k2}	time constants of the transient response during unloaded conditions, s
A and C	parameters for unloaded conditions, V
B and D	parameters for unloaded conditions, s^{-1}
E and G	parameters for unloaded conditions, V
F and H	parameters for unloaded conditions, s^{-1}
M and N	gains for the gain correction
L	gain for the time constant correction
T_{s1} and T_{s2}	settling times of the transient response, s

equations can be implemented and the parameters derived using electrical circuits [6]. Furthermore, the I–V information can be readily extracted from the electrical model.

The most simple electrical battery model is a circuit with a controlled voltage source in series with a resistor, however, due to the transient response characteristic associated with the electrochemical process of a rechargeable battery, a second type of electrical battery model called the voltage–resistance–capacitance (VRC) model has been developed. The VRC model is a circuit with a controlled voltage source in series with a resistor and a RC parallel network as used in [6–12]. The VRC model is improved by utilizing two RC parallel networks as proposed by Chen and Mora [3]. It is useful in characterizing both the short and long time transient responses of the electrochemical process. Circuit diagram of the VRC model with two RC parallel networks is shown in Fig. 1. The VRC model with two RC parallel networks has been shown to have achieved high accuracy [3,4,13,14].

The parameters for the VRC model have been identified based on the voltage curve for the unloaded condition. There has been a disagreement about parameter identification and Norian has pointed out that the parametric values for loaded, unloaded and charged conditions are not necessarily the same [8]. The parameters obtained from the unloaded conditions are not suitable for the voltage response under loaded conditions. Hence, the transient response correction should be added to the existing electrical battery model so that it can be used for $LiFePO_4$ batteries. The transient response correction technique is straightforward and therefore simplifies the process of parameter extraction. The technique can be used to improve the accuracy of the existing battery model.

In this paper, a battery model with different parametric values of RC parallel networks, for loaded and unloaded conditions, is developed using transient response correction. The quality of the developed battery model is validated using data obtained from actual battery.

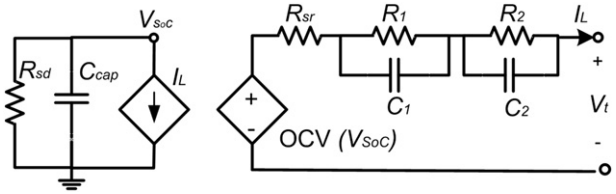

Fig. 1. Electrical battery model which proposed by Chen and Mora [3].

2. Improved model

Fig. 2 illustrates the proposed electrical battery model. It uses the same electrical circuit as the VRC model but with different parametric values of RC parallel networks for loaded and unloaded conditions. The terminal voltage and loaded current are represented by V_t and I_L respectively. The open-circuit voltage (OCV) is represented by a voltage source which is dependant on the state-of-charge (SoC) of the battery. SoC represents the remaining capacity of the battery as denoted by Eq. (1) where $\gamma(t_k)$ is the SoC at time t_k, $\gamma(t_0)$ is the initial SoC and C_N is nominal capacity of the battery.

$$\gamma(t_k) = \gamma(t_0) - \frac{1}{C_N}\int_{t_0}^{t_k} I_L(t)dt \quad , t_0 < t < t_k \tag{1}$$

The series resistance of the battery is characterized by both R_{sr} and R_a. R_{sr} is used to represent the series resistance when the battery is fully charged and its value is constant, however, the series resistance is found to be larger when the battery is loaded under partially charged conditions. Hence, a resistor R_a is used to represent the increment in the series resistance. In this formulation, the value of R_a is dependant on the initial SoC when the battery is loaded and the value of R_a is zero when the battery is fully charged (SoC=100%).

The transient characteristic of the battery's electrochemical process is characterized by using two RC parallel networks. For loaded conditions, the parameters of RC parallel networks are R_1, R_2, C_1 and C_2 as shown in Fig. 2(a) whereas the parameters of RC parallel networks are, R'_1, R'_2, C'_1 and C'_2 for unloaded conditions as shown in Fig. 2(b). The details on parameter identification are discussed in Section 4.

3. Experiment set up and procedures

3.1. Experiment set up

The block diagram and the experiment set-up for the battery test are shown in Figs. 3 and 4. The test system consists of a $LiFePO_4$

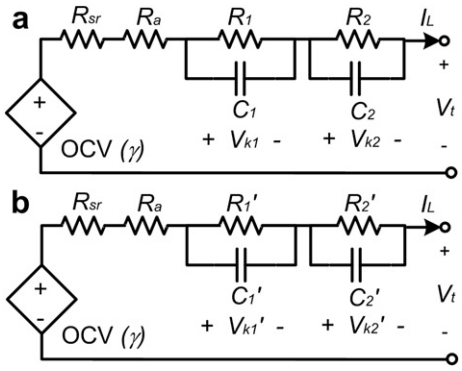

Fig. 2. Proposed electrical battery model for (a) loaded conditions and (b) unloaded conditions.

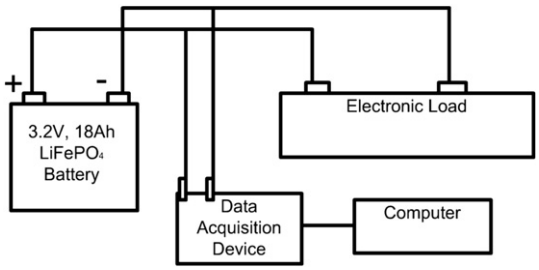

Fig. 3. Block diagram of battery tests.

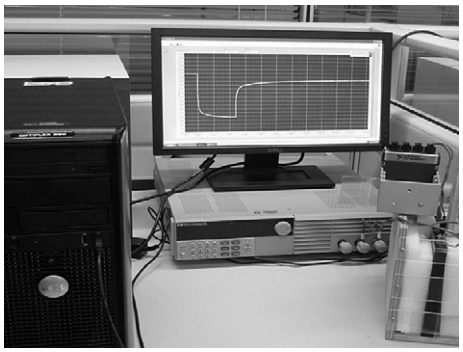

Fig. 4. Equipment set-up of battery tests.

battery, whose nominal capacity and nominal voltage are 18 Ah and 3.2 V respectively. The DAQ NI9219 which produced by National Instruments is interfaced with LabVIEW 2010 and a computer to collect data from the experiment. The battery tests, which require a constant current load, are carried out by using electronic load IT8514C (produced by ITECH) with ratings of 120 V, 240 A and 1200 W.

3.2. Battery test procedure

Pulse discharge (PDT) and continuous discharge (CDT) tests are performed on the $LiFePO_4$ battery for parameter identification and model validation. The PDT test consists of a sequence of constant current discharge and rest periods. The battery is loaded with 9 A (0.5 C) of current for 720 s to reduce 10% of the battery's SoC. After 4 h of rest, the same discharge pulse is applied until the battery voltage reaches 2.0 V. In this configuration, the battery is unloaded for a long

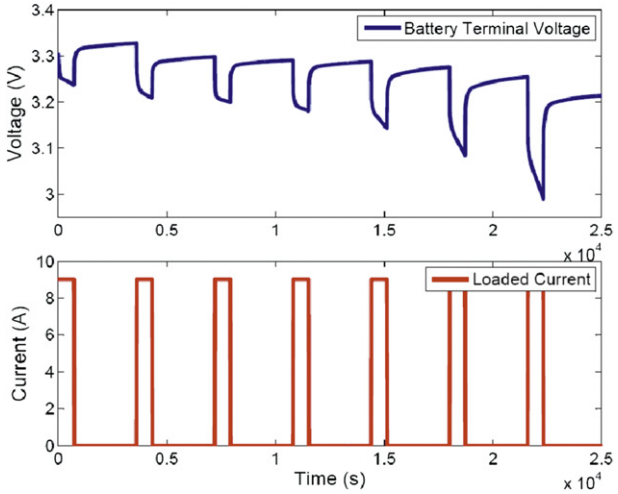

Fig. 5. Voltage response and current profile for PDT test.

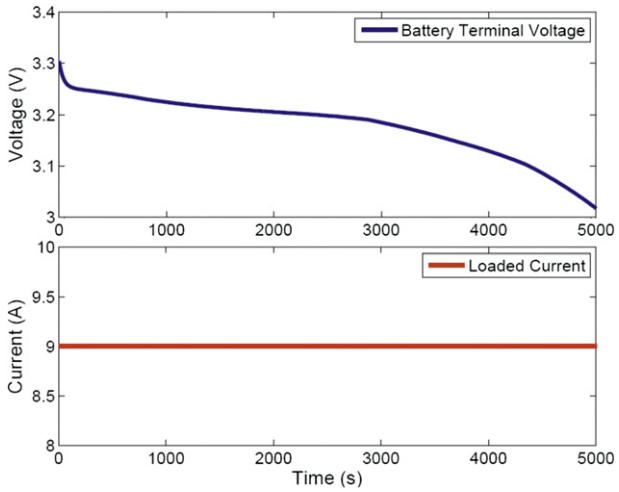

Fig. 6. Voltage response and current profile for CDT test.

period (10 times longer than the RC transient) to accurately determine the parameters of the battery model as suggested in [15]. In this modelling technique, battery is required to be in full relaxed condition, thus highly transient current is not suitable for parameter identification. Also, in order to avoid permanent damage caused by over usage, the battery voltage is strictly controlled to be higher than 2.0 V. Several PDT tests are carried out with different current pulses in order to investigate the parameters for several current loads. On the other hand, the CDT test is done by discharging the battery with continuous constant current. Continuous discharge tests for 9 A (0.5 C), 13.5 A (0.75 C) and 18 A (1 C) of current are made. The typical voltage response and the current profile for PDT and CDT battery tests are shown in Figs. 5 and 6 respectively.

4. Model extraction and transient response correction

In the developed model, all the parameters are expressed as a function of SoC. Because the value of SoC is decreasing during loaded conditions, the identification of parametric equations is difficult. Therefore, the model extraction is initiated from the unloaded conditions with a constant value of SoC. After the values of parameters are determined from the unloaded conditions, a transient response correction is employed in order to determine the value of parameters for the loaded conditions.

4.1. Parameter identification for the unloaded conditions

As seen in Fig. 2(a), the value of loaded current, I_L, is zero for the unloaded conditions. Consequently, the values of series resistances R_{sr} and R_a are not important for the unloaded conditions. The

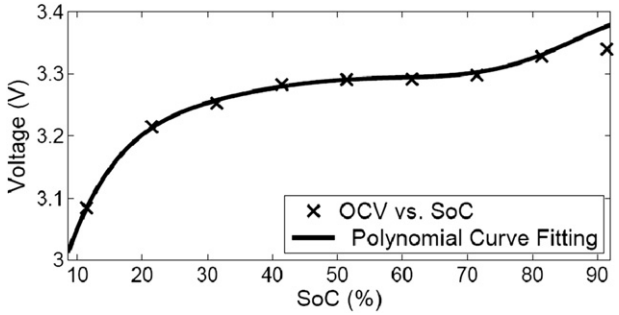

Fig. 7. OCV–SoC relationship.

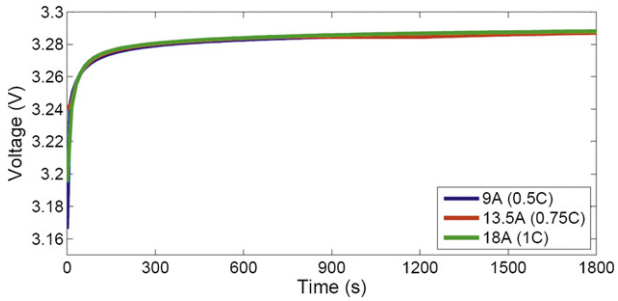

Fig. 8. Relaxation curve at 80% SoC for 9 A (0.5 C), 13.5 A (0.75 C) and 18 A (1 C) PDT tests.

terminal voltage, V_t, is denoted as Eq. (2). V'_{k1} and V'_{k2} are the voltages across the RC parallel networks during the unloaded condition, whereas $V_{k1}(\alpha)$ and $V_{k2}(\alpha)$ are the voltage levels across the RC parallel networks at the beginning of unloaded condition, α. τ'_{k1} and τ'_{k2} represent the time constants of the transient response of V'_{k1} and V'_{k2} respectively. In this paper, the parameter identification is done using MATLAB curve-fitting tools.

$$\begin{aligned} V_t(t) &= \mathrm{OCV}[\gamma(t)] - V'_{k1}(t) - V'_{k2}(t) \\ V'_{k1}(t) &= V_{k1}(\alpha)\exp\left(\frac{-(t-\alpha)}{\tau'_{k1}}\right) \quad , t>\alpha \\ V'_{k2}(t) &= V_{k2}(\alpha)\exp\left(\frac{-(t-\alpha)}{\tau'_{k2}}\right) \end{aligned} \tag{2}$$

where,

$$\tau'_{k1} = R'_1 \times C'_1, \tau'_{k2} = R'_2 \times C'_2$$

4.1.1. Open-circuit voltage, OCV

OCV for a certain SoC is determined by the terminal voltage of the battery after the battery is unloaded for a long period. As suggested in [15], the OCV can be precisely determined after the battery is unloaded for at least 10 times the time of the RC transient response. In this paper, the OCV is determined after the battery is at rest for 4 h. The OCV–SoC curve is shown in Fig. 7 and the relationship is expressed by Eq. (3), where γ represents SoC.

$$\begin{aligned} \mathrm{OCV}(\gamma) = &\left(-3.001\times10^{-11}\right)\gamma^6 + \left(9.85\times10^{-9}\right)\gamma^5 \\ &- \left(1.291\times10^{-6}\right)\gamma^4 + \left(8.763\times10^{-5}\right)\gamma^3 \\ &- 0.003325\gamma^2 + 0.07002\gamma + 2.607 \end{aligned} \tag{3}$$

4.1.2. Parameters of transient response for the unloaded conditions

The voltage response for the unloaded condition is a combination of the transient responses having both a short time and long time constant. In this paper, two RC parallel networks are used to represent the voltage responses. In order to simplify the modelling method, the equations for V'_{k1} and V'_{k2} can be expressed as Eq. (4), where A, B, C, and D represent the desired values of $V_{k1}(\alpha)$, τ'^{-1}_{k1}, $V_{k2}(\alpha)$ and τ'^{-1}_{k2} respectively. Thus, the parameter identification of R'_1, R'_2, C'_1 and C'_2 can be avoided. It is important to note that the parameters A, B, C and D are independent of discharge current, I_L, since the relaxation curves, as shown in Fig. 8, are similar for all current rates.

$$\begin{aligned} V'_{k1}(t) &= A\exp(-B(t-\alpha)) \\ V'_{k2}(t) &= C\exp(-D(t-\alpha)) \end{aligned}, t>\alpha \tag{4}$$

where,

$$A = V_{k1}(\alpha), C = V_{k2}(\alpha)$$

$$B = \frac{1}{\tau'_{k1}}, D = \frac{1}{\tau'_{k2}}$$

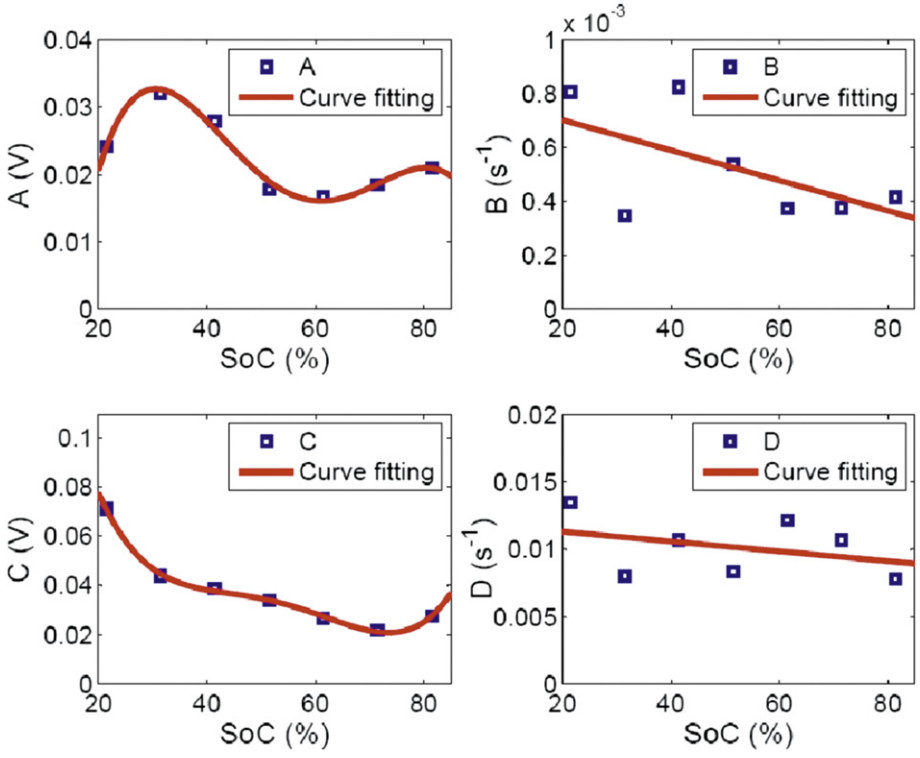

Fig. 9. Extracted parameters for unloaded conditions.

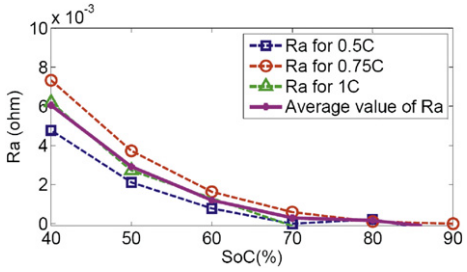

Fig. 10. R_a–SoC relationship.

This trend indicates that the process of parameter extraction for *A*, *B*, *C* and *D* is straightforward. The curve of parameters versus SoC is shown in Fig. 9. The identified parameters can be expressed by Eq. (5). The goodness-of-fit statistics of the curve fitting is tabulated in Table 1.

$$\begin{aligned} A(\gamma) &= -(2.5348\times10^{-8})\gamma^4 + (5.8161\times10^{-6})\gamma^3 - (4.6837\times10^{-4})\gamma^2 + (1.5226\times10^{-2})\gamma - 0.13906 \\ B(\gamma) &= -(5.6107\times10^{-6})\gamma + (8.1434\times10^{-4}) \\ C(\gamma) &= (3.9383\times10^{-8})\gamma^4 - (8.3679\times10^{-6})\gamma^3 + (6.4756\times10^{-4})\gamma^2 - (2.212\times10^{-2})\gamma + 0.32153 \\ D(\gamma) &= -(3.6536\times10^{-5})\gamma + 0.012037 \end{aligned} \quad (5)$$

4.2. Parameter identification for the loaded conditions

The voltage response of the loaded conditions consists of an instantaneous voltage drop and a series of transient responses. In this context, because the loaded current is not zero, the series resistances, R_{sr} and R_a must be determined. The terminal voltage, V_t, can be expressed by Eq. (6). V_{k1} and V_{k2} are the voltages across the RC parallel networks during the loaded condition while τ_{k1} and τ_{k2} represent the time constants of the transient response of V_{k1} and V_{k2} respectively. The parameters of the transient responses are then identified using a transient response correction technique.

$$V_t(t) = \mathrm{OCV}[\gamma(t)] - V_{k1}(t) - V_{k2}(t) - I_L(t)\times(R_{sr}+R_a)$$

where,

$$\begin{aligned} V_{k1}(t) &= I_L(t)\times R_1\left(1-\exp\left(\frac{-(t-t_0)}{\tau_{k1}}\right)\right) \\ V_{k2}(t) &= I_L(t)\times R_2\left(1-\exp\left(\frac{-(t-t_0)}{\tau_{k2}}\right)\right) \end{aligned}, t_0 < t < \alpha \quad (6)$$

and,

$$\tau_{k1} = R_1\times C_1, \tau_{k2} = R_2\times C_2$$

Table 1
Goodness-of-fit of curve fitting.

Goodness-of-fit	A	B	C	D
SSE	3.758×10^{-6}	1.7×10^{-7}	2.688×10^{-6}	2.551×10^{-5}
R-square	0.9811	0.3415	0.9984	0.1278
Adjusted R-square	0.9432	0.2098	0.9951	−0.04,665
RMSE	0.001371	0.0001844	0.001159	0.002259

4.2.1. Series resistances, R_{sr} and R_a

The series resistance is represented by both R_{sr} and R_a where R_{sr} represents the series resistance for a fully-charged battery and R_a represents the increment of series resistance for other SoC. Series resistance can be calculated from the instantaneous voltage drop when the load is applied. For this paper, the value of R_{sr} is 0.005889 Ω while the R_a is varied with SoC as shown in Fig. 10. The average value of R_a can be expressed by Eq. (7).

$$R_a[\gamma] = 0.1457e^{-0.07936\gamma} \quad (7)$$

4.2.2. Parameters of transient response for the loaded conditions

The terminal voltage, V_t, of the battery for the loaded conditions can be expressed by equation (6). During the loaded conditions, the SoC of the battery, γ, will decrease. Because all the parameters of transient response are dependant on the SoC, the functions for $V_{k1}(\gamma)$, $V_{k2}(\gamma)$, $\tau_{k1}(\gamma)$ and $\tau_{k2}(\gamma)$ cannot be accurately determined from the voltage curve. The transient response correction must be applied to determine the value of the parameters. An alternative way to determine parameters for loaded conditions is optimisation technique as discussed in [16–18]. Generic algorithm is applied in optimisation technique to generate parameter set for loaded condition, however, in transient response correction, the parameter identification is straightforward. The equations for V_{k1} and V_{k2} are simplified as Eq. (8).

$$\begin{aligned} V_{k1}(t) &= E(1-\exp(-F(t-t_0))) \\ V_{k2}(t) &= G(1-\exp(-H(t-t_0))) \end{aligned}, t_0 < t < \alpha \quad (8)$$

where,

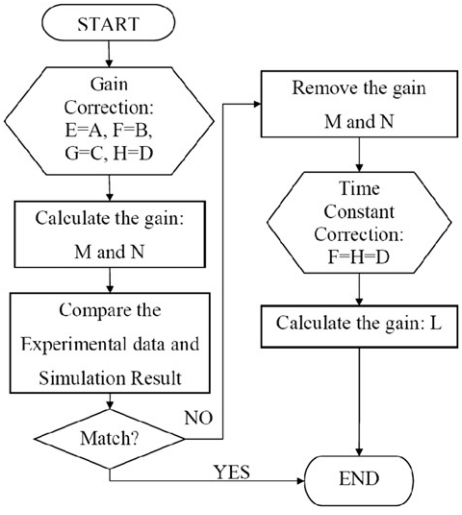

Fig. 11. Flow chart of transient response correction.

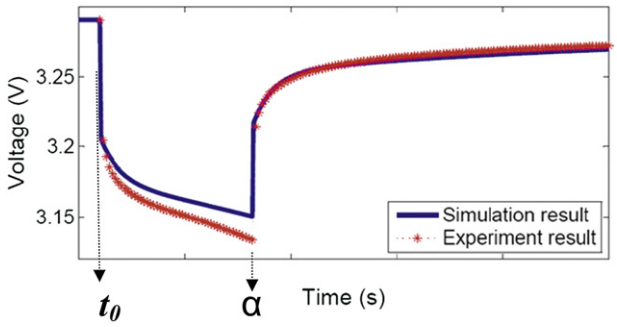

Fig. 12. Mismatch between experiment data and simulation result when the setting of $E = A$, $F = B$. $G = C$, and $H = D$.

$$E = I_L(t) \times R_1, G = I_L(t) \times R_2$$

$$F = \frac{1}{\tau_{k1}}, H = \frac{1}{\tau_{k2}}$$

4.2.3. Transient response correction method

The flow chart of the transient response correction method is shown in Fig. 11. The steps of the transient response correction method are as described as below.

4.2.3.1. Gain correction. The gain correction is started by assuming that the transient response parameters for the loaded conditions E to H have the same value as A to D. Because the values of $V_{k1}(t_0)$ and $V_{k2}(t_0)$ for the loaded condition are unknown, they are set to zero whilst the values of $V_{k1}(\alpha)$ and $V_{k2}(\alpha)$ are set to A and C,

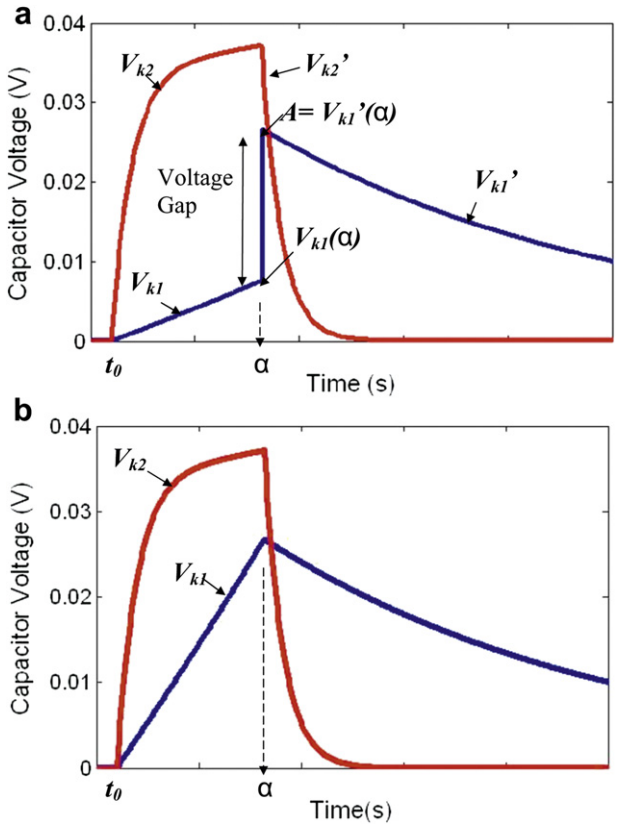

Fig. 13. Voltage curve of V_{k1} and V_{k2} (a) before and (b) after gain correction.

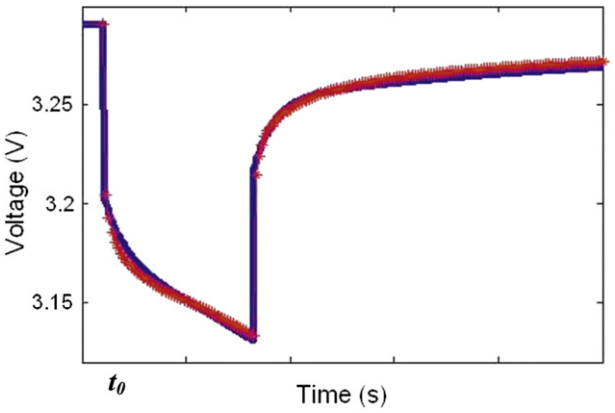

Fig. 14. Comparison between experiment data and simulation result after gain correction, with the setting of $E = M \times A$, $F = B$, $G = N \times$ C and $H = D$.

respectively, for the unloaded conditions. An example of mismatch between experiment and simulation results is shown in Fig. 12. The mismatch between experiment and simulation results proves that the parameters of transient response for loaded and unloaded conditions are not the same. Therefore, a transient response correction method is needed.

In order to perform a transient response correction, the voltage across the RC parallel networks is measured. Voltage responses for the voltage across the RC parallel networks before and after the transient response correction are shown in Fig. 13. Because the voltage curves of V'_{k1} and V'_{k2} represent the desired voltage curve for the voltage across the RC parallel networks in the relaxation condition, the V_{k1} and V_{k2} curves should match the curves of V'_{k1} and V'_{k2} at time α, however, as can be seen in Fig. 13(a), a voltage gap between V_{k1} and V'_{k1} is found. In order to meet the desired value of "A" during the unloaded condition, the value of $V_{k1}(\alpha)$ should be increased to the value of "A". The correction can be made by multiplying the value of E with a gain, M, as shown in Eq. (9). In Fig. 13(a), there is no voltage gap for V_{k2}, however, the same concept is applied by multiplying G with the gain of N if a voltage gap exists between V_{k2} and V'_{k2}. The value of R_1 and R_2 are determined by using equation (10) after the value of E and G are updated to E_{new} and G_{new} respectively. The mismatch between experimental and simulation results can be effectively solved as shown in Fig. 14.

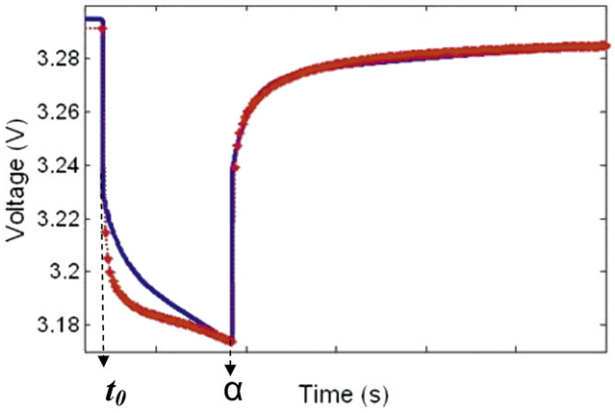

Fig. 15. Example of mismatch between experiment data and simulation result after the gain correction.

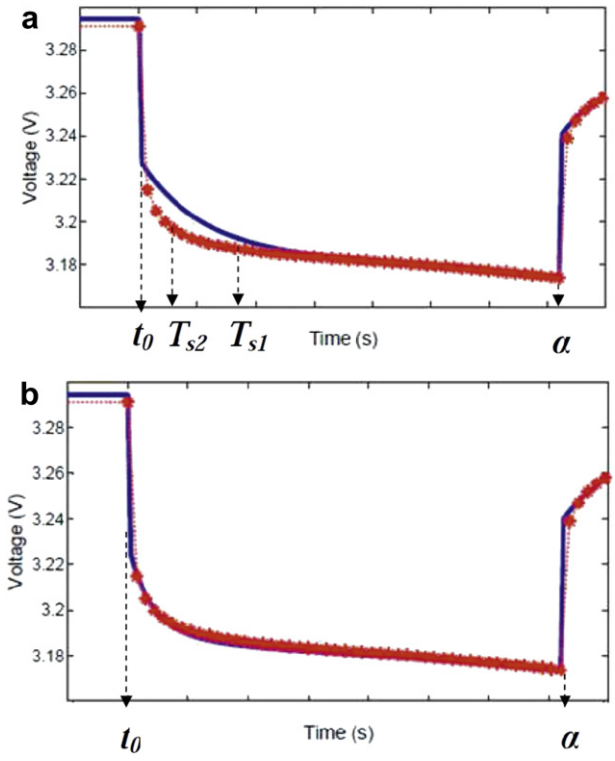

Fig. 16. Comparison between experiment data and simulation result (a) before and (b) after time constant correction, with the setting of $E = A$, $F = L \times D$, $G = C$ and $H = L \times D$.

$$E_{\text{new}} = M \times E = M \times A = \frac{V'_{k1}(\alpha)}{V_{k1}(\alpha)} \times A = I_L(t) \times R_1$$
$$G_{\text{new}} = N \times G = N \times C = \frac{V'_{k2}(\alpha)}{V_{k2}(\alpha)} \times C = I_L(t) \times R_2 \quad (9)$$

Therefore,

$$R_1 = \frac{E_{\text{new}}}{I_L(t)}$$
$$R_2 = \frac{G_{\text{new}}}{I_L(t)} \quad (10)$$

4.2.3.2. Time constant correction. Example of the mismatch between experiment and simulation results after the gain corrections is shown in Fig. 15. In this paper, this type of mismatch can be found at the high SoC region (SoC more than 60%). As can be seen, although the voltage curve of the experiment data and simulation result meet at the same point at time α, the rate of voltage drop is different. The rate of voltage drop for the experiment data is faster than the simulation result implying a deviation in the time constant. Hence, a time constant correction is made by shortening the time constant value of the transient response.

Table 2
The average value of correction gains in several SoC.

SoC (%)	M	N	L
$90 < \gamma < 100$			3.1667
$80 < \gamma < 90$			1.6
$70 < \gamma < 80$			2.4
$60 < \gamma < 70$			1.5
$50 < \gamma < 60$	3.51,693	1.01,228	
$40 < \gamma < 50$	2.9898	1.036	
$\gamma < 40$	2.1	1.00,944	

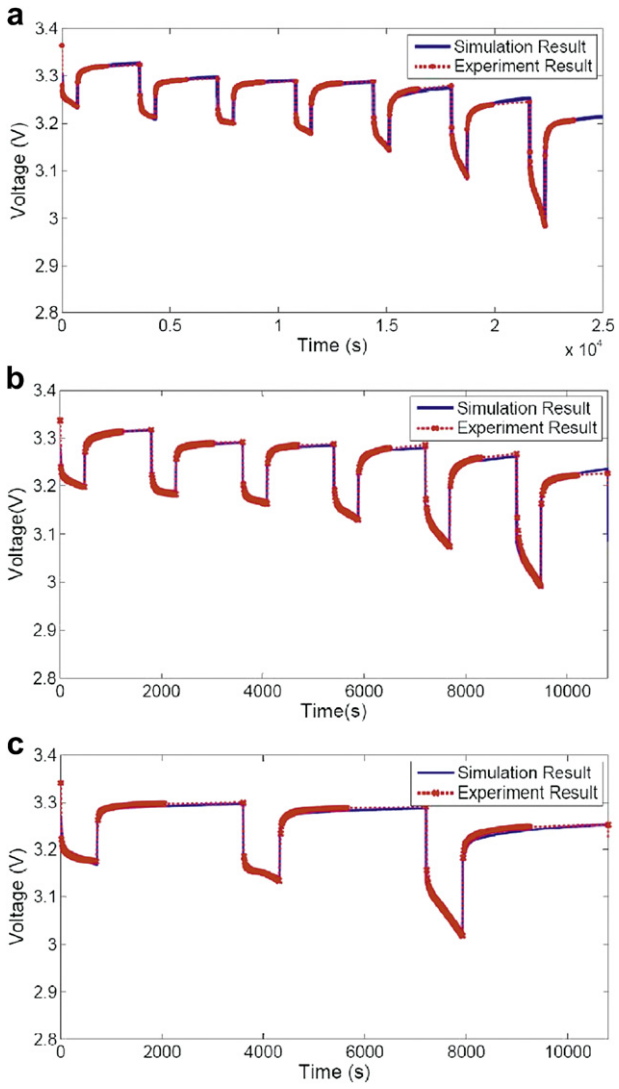

Fig. 17. Comparison between simulation result with the experiment data of PDT test for (a) 9 A (0.5 C), (b) 13.5 A (0.75 C) and (c) 18 A (1 C).

The time constant correction is started by removing the gain corrections, M and N. Then, the time constant correction is made by setting both τ_{k1} and τ_{k2} to be equal to the value of the shorter time constant in the unloaded condition, τ'_{k2}. The values of F and H are set to be equal to D and the transient response of the battery has now become first order.

Processes of time constant correction are illustrated in Fig. 16. After the time constant is set to D^{-1}, the comparison between experiment and simulation results is made as shown in Fig. 16(a). The comparison shows that the settling time of the transient response is different. The correction of the time constant is made by using a time constant gain, L, as expressed in Eq. (10). The result of the comparison after the time constant correction is shown in Fig. 16(b). The result shows that the correction effectively solves the problem of time constant mismatch.

Table 3
RMS modelling errors in PDT tests.

Current (A)	RMS error (V)
9	0.0035
13.5	0.0116
18	0.0079

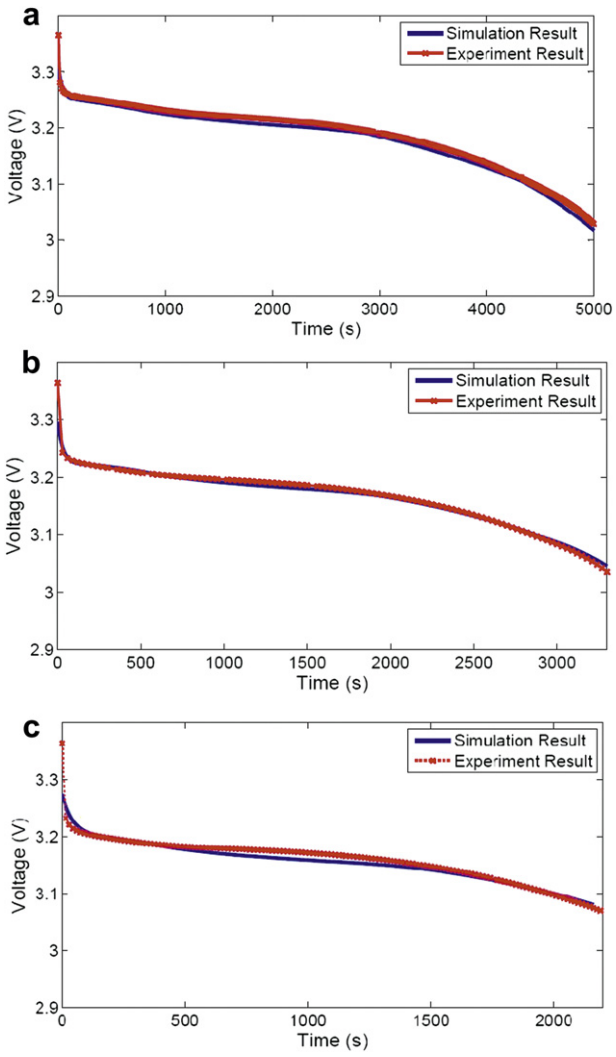

Fig. 18. Comparison between simulation result and experiment data of CDT test for (a) 9 A (0.5 C), (b) 13.5 A (0.75 C) and (c) 18 A (1 C).

$$F = H = L \times D = \left(\frac{T_{s1} - t_0}{T_{s2} - t_0}\right) \times D \tag{11}$$

Average values of gain correction in several SoC for the loaded current between 9 A (0.5 C) to 18 A (1 C) is tabulated in Table 2. For this case, it was found that the time constant correction is imperative for the SoC region higher than 60% whereas the gain correction is applied for the SoC region of 60% and below.

5. Model validation

In order to validate the developed model, the experiment data of PDT and CDT tests are compared with the simulation results. Comparison between experiment data and with the simulation result of the PDT tests is shown in Fig. 17. The load profiles are:

Table 4
RMS modelling errors in CDT tests.

Current (A)	RMS error (V)
9	0.0094
13.5	0.0124
18	0.0125

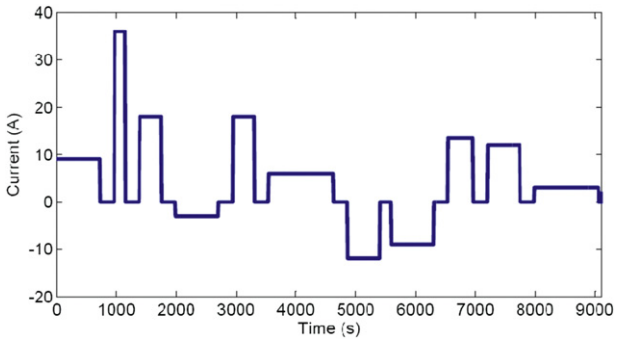

Fig. 19. Current profile in random pulse test.

(a) 9 A (0.5 C) constant current pulse with a 720 s duty cycle and a period of 1 h per cycle. (10% of SoC reduction per cycle).
(b) 13.5 A (0.75 C) constant current pulse with a 480 s duty cycle and a period of 30 min per cycle. (10% of SoC reduction per cycle).
(c) 18 A (1 C) constant current pulse with a 720 s duty cycle and a period of 1 h per cycle. (20% of SoC reduction per cycle).

There is a close agreement between experiment and simulation results as shown in Fig. 17. The 0.03 V of maximum error for the PDT tests is found at the beginning of discharging (within a short time). As discussed in Section 4.2.3.2, the RC transient responses are adjusted to be first order when the time constant correction is made. Therefore, the simulation result is slightly different from the experiment data due to the small deviation between first order and second order transient responses. The RMS modelling errors in PDT tests are tabulated in Table 3.

On the other hand, the comparison between experiment and simulation results for several CDT test are shown in Fig. 18. The comparative analysis shows that experiment and simulation results are well matched. The maximum error, which happens at the beginning of discharging, is 0.018 V and is caused by the small deviation between first order and second order transient responses. The RMS modelling errors in CDT tests are tabulated in Table 4.

The developed model is further validated with random pulse test. In this test, battery is loaded with various current rates as shown in Fig. 19, which including 3 A (0.1667 C), 6 A (0.3333 C), 12 A (0.6667 C), and 36 A (2 C) of current. Moreover, some of the charging conditions are also included in the test. The comparison between experiment and simulation results for random pulse test is shown in Fig. 20. The comparative analysis shows that experiment and simulation results are well matched with RMS modelling error of 0.0189 V.

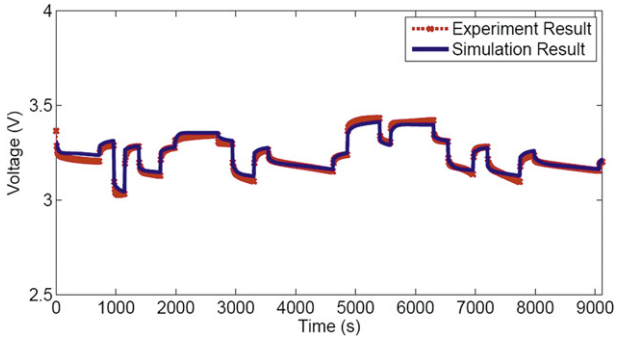

Fig. 20. Comparison between simulation result and experiment data of random pulse test.

Based on the good match between experiment and simulation results, the developed model is validated. This proves that the transient response correction technique is capable of reducing the mismatch between the model and the experiment data.

6. Conclusions

In this paper, an accurate and simple electrical battery model is successfully developed. The modification, to include the transient response, of an existing electrical battery model is successfully applied to reduce the modelling error in both loaded and unloaded conditions. The close agreement between simulation and experiment results shows that the characteristics of a $LiFePO_4$ battery can be accurately simulated with the developed model. Moreover, the simple approaches in model extraction enable the researcher to easily build up a higher accuracy battery model. With the proposed model, the battery modelling method can be simplified and will eventually help in the development of battery management systems and energy storage systems for green technology applications.

Acknowledgements

This work was supported by MoHE (Ministry of Higher Education) under the Fundamental Research Grant Scheme (FRGS) of Malaysia and Universiti Teknologi Malaysia under the project "Fundamental Study of Electric Vehicle Charging System" (Vot No: 78492).

References

[1] M. Urbain, M. Hinaje, S. Rael, B. Davat, P. Desprez, IEEE Trans Energy Conversion 25 (3) (2010) 862–872.
[2] C. Liao, Z. Tang, L. Wang, Proceedings of the 2010 Asia-Pacific Power and Energy Engineering Conference, 2010, pp. 1–4.
[3] M. Chen, G.A.R. Mora, IEEE Trans Energy Conversion 21 (2) (2006) 504–511.
[4] J. Zhang, S. Ci, H. Sharif, M. Alahmad, IEEE Trans Energy Conversion 25 (4) (2010) 1133–1141.
[5] K.M. Tsang, L. Sun, W.L. Chan, Energy Conversion and Management 51 (2010) 2857–2862.
[6] I.S. Kim, Journal of Power Sources 163 (2006) 584–590.
[7] W. Y. Low, J. A. Aziz, Proceedings of the 2011 Applied Power Electronics Colloquium, 2011, pp. 104–109.
[8] K.H. Norian, Journal of Power Sources 196 (2011) 2360–2363.
[9] L. Gao, S. Liu, R.A. Dougal, IEEE Trans Component and Packing Technologies 25 (3) (2002) 495–505.
[10] J. Kim, J. Shin, C. Jeon, B. Cho, Proceedings of the 26th Annual IEEE Applied Power Electronics Conference and Exposition, 2011, pp. 1984–1991.
[11] S. Lee, J. Kim, J. Lee, B.H. Cho, Journal of Power Sources 185 (2008) 1367–1373.
[12] R. Benger, H. Wenzl, H.P. Beck, M. Jiang, D. Ohms, G. Schaedlich, World Electric Vehicle Journal 3 (2009) 1–10.
[13] C. Liao, H. Li, L. Wang, Proceedings of the 2009 IEEE Vehicle Power and Propulsion Conference, 2009, pp. 1662–1665.
[14] O. Erdinc, B. Vural, M. Uzunoglu, Proceedings of the 2009 International Conference on Clean Electrical Power, 2009, pp. 383–386.
[15] H. Zhang, M. Chow, IEEE Power and Energy Society General Meeting, Minneapolis, 2010, pp. 1–6.
[16] Y. Hu, S. Yurkovich, Y. Guezennec, B.J. Yurkovich, Control Engineering Practice 17 (2009) 1190–1201.
[17] Y. Hu, S. Yurkovich, Y. Guezennec, B.J. Yurkovich, Journal of Power Sources 196 (2011) 449–457.
[18] X. Hu, S. Li, H. Peng, Journal of Power Sources 198 (2012) 359–367.